ISPRS Journal of Photogrammetry and Remote Sensing 169 (2020) 17–28

Contents lists available at ScienceDirect

ISPRS Journal of Photogrammetry and Remote Sensing

journal homepage: www.elsevier.com/locate/isprsjprs

Retrieving snow wetness based on surface and volume scattering simulation

Wei Ma [a], Pengfeng Xiao [a,b,*], Xueliang Zhang [a], Yina Song [a], Tengyao Ma [a], Lizao Ye [a]

[a] Jiangsu Provincial Key Laboratory of Geographic Information Science and Technology, Key Laboratory for Land Satellite Remote Sensing Applications of Ministry of Natural Resources, School of Geography and Ocean Science, Nanjing University, Nanjing, Jiangsu 210023, China
[b] Jiangsu Center for Collaborative Innovation in Geographical Information Resource Development and Application, Nanjing, Jiangsu 210023, China

ARTICLE INFO

Keywords:
Snow wetness
Scattering simulation
Polarimetric decomposition
GaoFen-3
Radarsat-2

ABSTRACT

Wetness is one of the important physical parameters of snowpack. Its spatial and temporal changes play a key role in snowmelt runoff forecast, regional climate change, and agricultural irrigation. In this study, we proposed a new method to retrieve snow wetness from full-polarimetric synthetic aperture radar (SAR) data. First, the dominant scattering components, i.e. surface and volume scattering, in wet-snow conditions were obtained by polarimetric decomposition. The random rough surface scattering models and the dense media radiative transfer (DMRT) model were then used to establish the surface and volume scattering models, through which the surface and volume scattering lookup tables were created, respectively. Based on the lookup tables and the polarimetric decomposition results, the snow surface and volume wetness were retrieved, respectively. Finally, the effective snow wetness was derived from the weighted summation of surface and volume wetness. The advantage of this method mainly comes from the full consideration the snow surface roughness, the local incidence angle on complex mountain terrain, and the polarimetric information. In experiments, the GaoFen-3 data obtained on January 17, 2018 in the Kelan River Basin and the Radarsat-2 data obtained on March 19, 2014 in the Manasi River Basin were selected to verify the applicability of the proposed method at different conditions. From the analysis of experiment results, the correlation coefficient between the estimated and the ground measured snow wetness in the Kelan River Basin is 0.72. The mean absolute error (MAE) and the root mean square error (RMSE) are 3.35% and 3.89%, respectively. The correlation coefficient between the snow wetness estimated by Radarsat-2 and the measured values in the Manasi River Basin is 0.62. MAE and RMSE are 1.32% and 1.62%, respectively. These results proved that the proposed method can effectively retrieve snow wetness under different SAR data, different areas, and different snow periods.

1. Introduction

As one of the most active factors in the cryosphere, snow on the Earth's surface impacts human in many direct and indirect ways (Shi et al., 1993). Especially in alpine regions, the snowpack and its seasonal changes play an important role in ecological environment and human activities (Rondeau-Genesse et al., 2016). The condensation and melting of snow is companied by the release and absorption of energy, which significantly affects water circulation and regional climate (Cui et al., 2017; Shi and Dozier, 1995). Moreover, snow and glacier meltwater is the main source for agricultural irrigation. Among the physical properties of snow, wetness is one of the important properties and necessary condition for the outflow of snowmelt water that indicates the beginning of snowmelt process. Obtaining the spatial and temporal distribution information of snow wetness is helpful to understand the mechanism of snow melting, which is of great significance to the prediction of snowmelt runoff and the allocation and management of water resources (Singh and Venkataraman, 2010a).

Active microwave remote sensing represented by synthetic aperture radar (SAR) provides a powerful way to inverse snow parameters (Singh and Venkataraman, 2010b). Microwave has long promised the advantages of sensitivity to many snow parameters that snow hydrologists use, especially free liquid water content in snowpack (Shi, 2001). For dry snow, SAR backscattering is mainly affected by the underlying surface due to the penetration of microwave. For wet snow, the backscattering mainly comes from the air-snow surface and the volume (Bhattacharya et al., 2014; Cui et al., 2017). In addition, the backscattering is affected by (1) the sensor parameters including the frequency, polarization, and

* Corresponding author at: Jiangsu Provincial Key Laboratory of Geographic Information Science and Technology, Key Laboratory for Land Satellite Remote Sensing Applications of Ministry of Natural Resources, School of Geography and Ocean Science, Nanjing University, Nanjing, Jiangsu 210023, China.
E-mail address: xiaopf@nju.edu.cn (P. Xiao).

https://doi.org/10.1016/j.isprsjprs.2020.08.021
Received 10 March 2020; Received in revised form 24 August 2020; Accepted 28 August 2020

viewing geometry, and (2) the snow parameters including snow surface roughness, snow density, snow wetness, and snow grain sizes and shapes (Yu et al., 2004). The complex relation between SAR backscattering and snow wetness makes it unrealistic to develop a simple and effective empirical relation between SAR signal and field measurements (Shi, 2001).

Several models for snow wetness inversion have been proposed using SAR data with different band and polarization. In 1993, Shi et al. (1993) developed an inversion model to estimate snow wetness based on the first-order scattering model when considering only the surface and volume scattering. In 1995, Shi and Dozier (1995) used the simplified surface scattering model and the relations between different polarizations to develop a new inversion model. In 2001, Shi (2001) established a model-simulated C-band database using multi-scattering model to decompose the surface and volume scattering, and then estimated snow wetness using each scattering component. Based on the physical optics model (POM), Singh et al. (2006) proposed a snow wetness inversion model for Envisat ASAR dual polarization data. Thereafter, Singh and Venkataraman (2007, 2010a) further developed the C- and X-band multi-polarization SAR inversion methods of snow wetness on the basis of Shi-Dozier model. In recent years, the full-polarimetric SAR data were used to establish new snow wetness inversion model based on polarimetric target decomposition technology. The surface and volume scattering components obtained by the polarimetric decomposition were correlated with the Bragg coefficients and Fresnel power transmission coefficients respectively to retrieve snow wetness (Surendar et al., 2013, 2015). The complex terrain of snow-covered areas in high mountains will lead to a wide range of local incidence angles. There is a positive correlation between snow surface roughness and microwave signals. For wet snow, backscattering is sensitive to snow surface roughness. Moreover, the role of cross-polarization terms in wetness inversion is often overlooked. The above models only take into account part of the influencing factors in snow wetness inversion. How to simultaneously consider the wide range of local incidence angles and snow surface roughness on mountain complex terrain and the role of cross-polarization terms remains unsolved.

In this study, we propose a new snow wetness inversion method using C-band full-polarimetric SAR data. This method fully considers the range of local incidence angle and snow surface roughness on complex terrain conditions in mountainous areas, which improves the applicability of the method. In addition, it also considers the role of cross-polarization terms in the inversion. The main component of this method is the establishment of surface and volume scattering models. Based on the two models, two lookup tables can be created by simulating the surface and volume scattering. Then we use the lookup tables and the surface and volume scattering obtained by polarimetric decomposition to calculate the surface and volume wetness, respectively. Finally, the effective snow wetness is derived from the weighted summation of the surface and volume wetness. Moreover, we select two types of study areas and SAR data to verify the applicability of the proposed method.

2. Study areas and data

2.1. Study areas

Xinjiang Province is one of the three largest snow cover areas in China. Altay, Tianshan, and Kunlun Mountains are distributed from north to south in Xinjiang Province. These mountains are the sources of

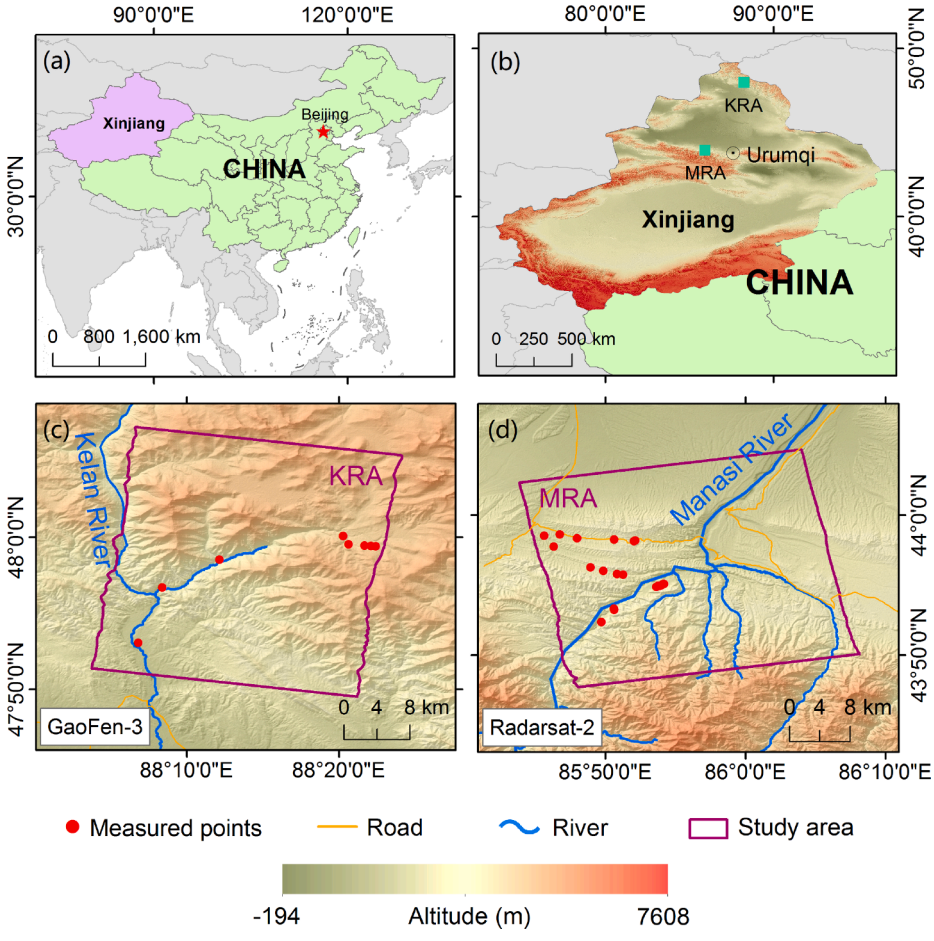

Fig. 1. Maps of the two study areas KRA (c) and MRA (d), located in Kelan River Basin and Manasi River Basin, Xinjiang Province (b), China (a), respectively.

many rivers, such as the Irtysh River, the Ili River, and the Tarim River. The melting snow and glaciers on these mountains provide an important supply for these rivers. Accordingly, we choose two areas as the study areas, one is located in the Altay Mountains and the other is located in the Tianshan Mountains (Fig. 1). There are differences in terrain and climate conditions between them. These differences not only lead to different snow characteristics, but also provide different conditions for the validation of the proposed method.

The area covered by GaoFen-3 satellite data lies in the southern piedmont of Altay Mountains, belonging to the Kelan River Basin (latitude 47°49′ N to 48°07′ N, longitude 88°03′ E to 88°24′ E). This area is abbreviated as KRA. The elevation in KRA decreases from north to south. The elevation difference is around 2500 m with an average elevation of 1174 m. The KRA has a temperate continental climate with an average annual temperature of 5.2 °C. The snow cover period starts from mid or late October and ends in late March or early April, and the snowfall accounts for 30–60% of the annual precipitation. The annual snow depth is greater than 40 cm (Zhuo et al., 2017).

The area covered by Radarsat-2 satellite data lies in the northern piedmont of Tianshan Mountains, belonging to the Manasi River Basin (latitude 43°47′ N to 44°04′ N, longitude 85°43′ E to 86°08′ E). This area is abbreviated as MRA. Contrary to the KRA, the elevation in MRA decreases from south to north. The elevation difference is around 2000 m with an average elevation of 2936 m. The MRA also belongs to the temperate continental climate with an average annual temperature of 6.5 °C. The annual snow depth is over 20 cm (Xiao et al., 2015).

2.2. Data

Considering the penetration characteristics of different wavelengths, two C-band full-polarimetric SAR data were selected to estimate the snow wetness. One is the GaoFen-3 satellite data in the Kelan River Basin, and the other is the Radarsat-2 satellite data in the Manasi River Basin. The detailed parameters of the SAR data are presented in Table 1. The data preprocessing mainly includes the polarimetric target decomposition and the backscattering coefficient extraction.

Field campaigns were conducted to collect near-real time in situ measurements according to the acquisition date of the GaoFen-3 and Radarsat-2 data, respectively. We obtained 8 measured points in the KRA and 17 measured points in the MRA, respectively (Fig. 1). Each snow pit was dug 20–80 cm in the KRA and 8–15 cm in the MRA. Snow wetness and density were measured using the Snow Fork instrument. Because the snow depth of the KRA was greater than that of the MRA, we measured snow wetness and density every 10 cm depth interval of the snowpack in the KRA and every 5 cm in the MRA measured. These measured points were used to validate the results of the proposed method. It is noted that selecting the wetness value in which layer for validation needs to be analyzed in conjunction with the C-band penetration depth, as presented in Section 4.4.

3. Method

Because of the different mechanism of snow surface scattering and volume scattering, wetness inversion first needs to obtain surface and volume scattering components under different snow conditions, and then perform the inversion separately based on different contribution values. In addition, due to the influence of different wetness, snow surface roughness, local incident angle, and other conditions, it will cause great differences in the scattering components (Fig. 2). The complexity of snow backscattering caused by the above factors prevents us from using simple inversion method to obtain snow wetness. This is an important reason why we propose the following method.

The flowchart in Fig. 3 illustrates the main steps of the proposed method.

Firstly, the surface scattering and volume scattering are obtained from the full-polarimetric SAR data through polarimetric target decomposition. Then, we use the random rough surface scattering models, the dense media radiative transfer (DMRT) model, and the Fresnel power transmission coefficients to establish the surface and volume scattering models. The established surface and volume scattering models are used to simulate the surface and volume scattering within a large parameter range. The simulated results can form the surface and volume scattering lookup tables that basically include SAR scattering values under general snow conditions. According to the local incidence angle generated by processing, snow surface roughness information obtained in the previous literature, and measured snow wetness values, the surface scattering lookup table includes a wide range of local incidence angles, snow surface roughness, and surface wetness parameters. The volume scattering lookup table includes a wide range of local incidence angles, volume scattering of HH polarization, and volume wetness parameters. Based on the lookup tables and the surface and volume scattering obtained by the polarimetric decomposition, the snow surface wetness (W_s) and volume wetness (W_v) can be calculated separately. Finally, the effective snow wetness (W_e) can be derived from the weighting summation of snow surface and volume wetness. The weights are derived from the surface (σ_Y^s) and volume (σ_Y^v) scattering powers obtained by the polarimetric decomposition:

$$W_e = \omega_s W_s + \omega_v W_v, \tag{1}$$

where ω_s and ω_v are the weights of the surface and volume wetness, respectively, and $\omega_s + \omega_v = 1$, $\omega_s = \sigma_Y^s/(\sigma_Y^s + \sigma_Y^v)$, $\omega_v = \sigma_Y^v/(\sigma_Y^s + \sigma_Y^v)$.

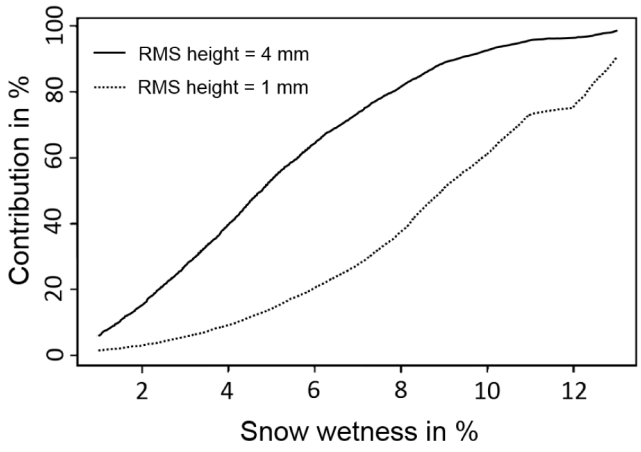

Fig. 2. Surface scattering contributions to total backscattering for two snow surface roughness conditions. Parameters are: ice volume fraction 0.36, ice particle radius 0.45 mm, root mean square (RMS) height 4 mm (solid line) and 1 mm (dotted line), snow surface correlation length 6 cm, and local incidence angle 40° (adopted from Shi and Dozier, 1995).

Table 1
Parameters of the SAR data.

Satellite	Date	Snow Cover Period	Azimuth Resolution (m)	Range Resolution (m)	Product Form	Pass
GaoFen-3	Jan. 17, 2018	Snow accumulation period	8	6–9	Single look complex	Descending
Radarsat-2	Mar. 19, 2014	Snow melting period	7.6	5.2–17.3	Single look complex	Ascending

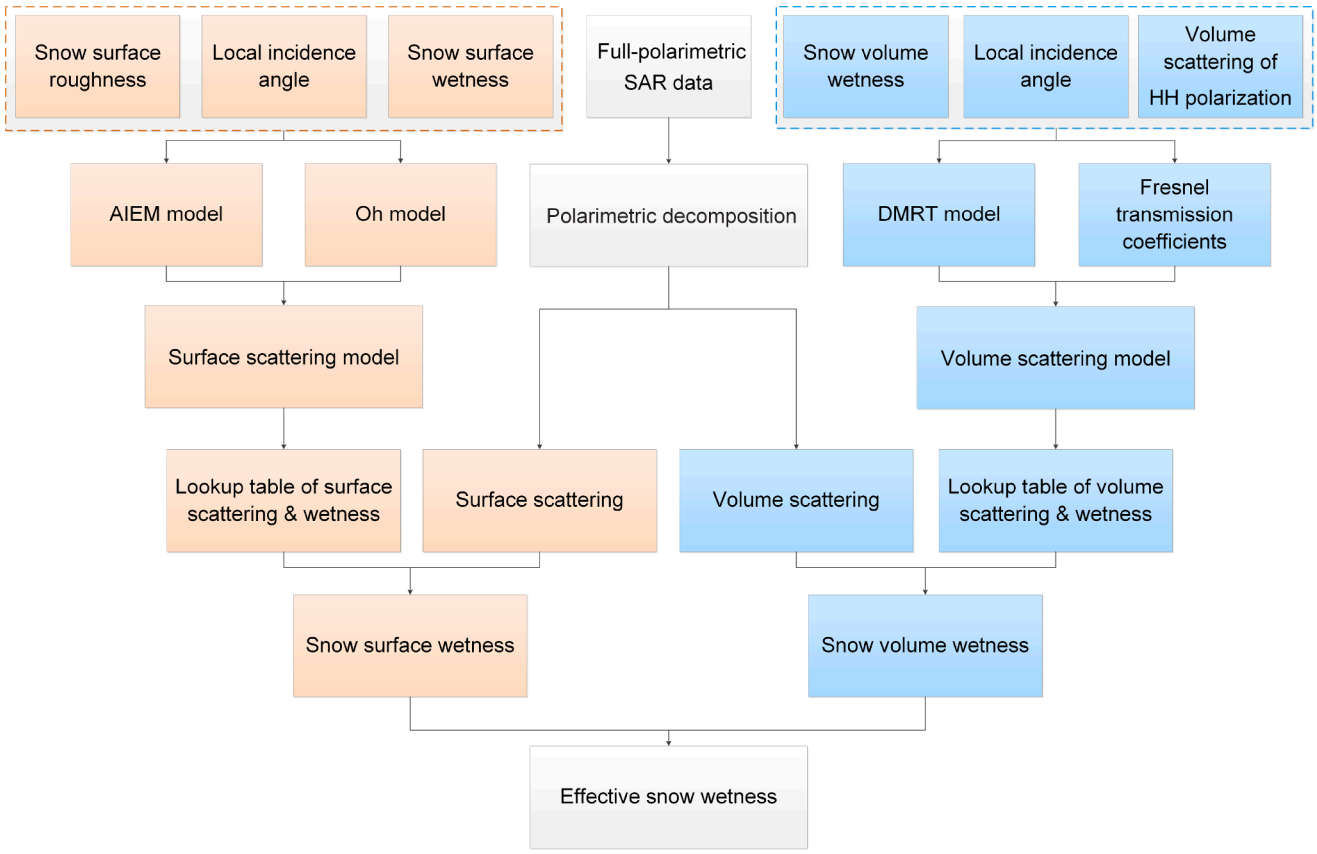

Fig. 3. Flowchart of the proposed snow wetness retrieval method.

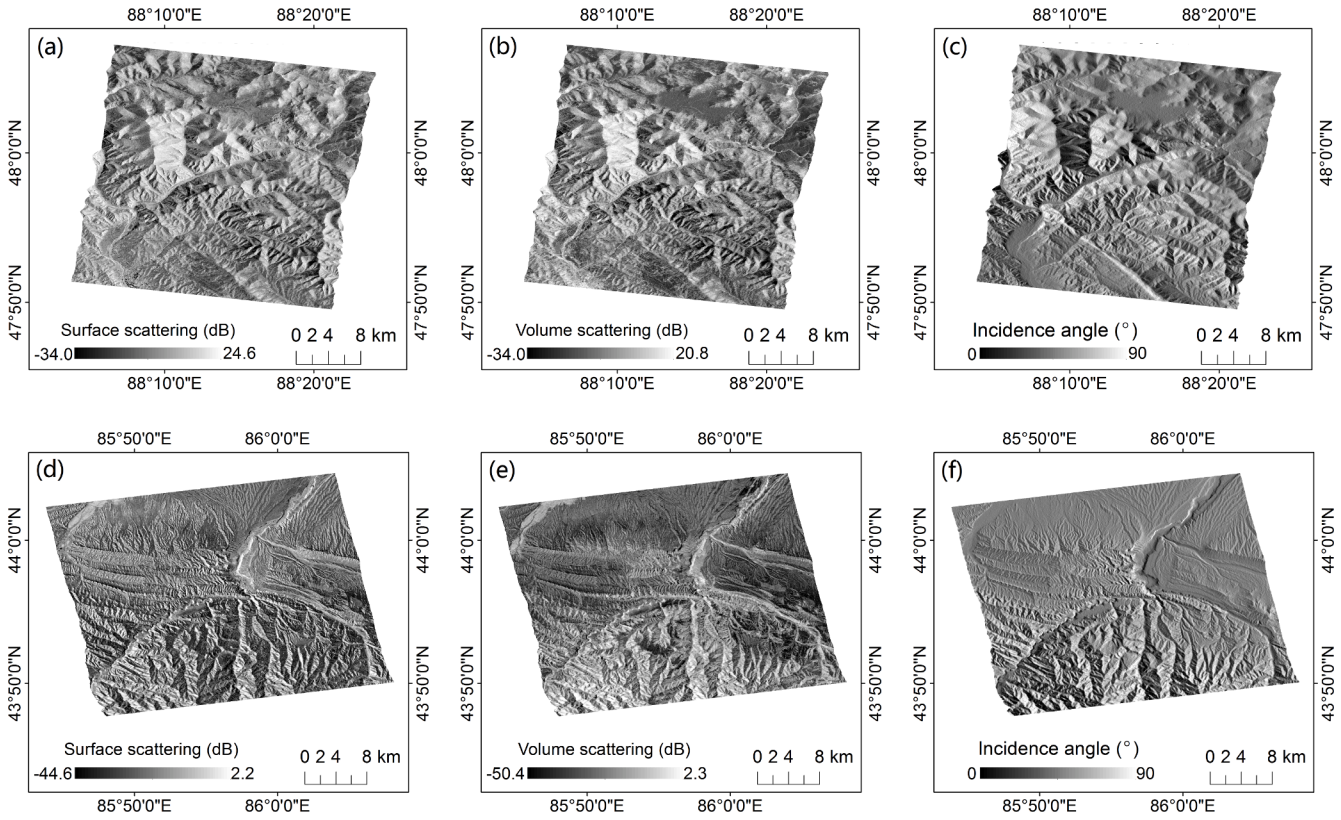

Fig. 4. Polarimetric target decomposition results of the Yamaguchi method and local incidence angle maps. (a) and (d) are surface scattering, (b) and (e) are volume scattering, and (c) and (f) are local incidence angle of GaoFen-3 and Radarsat-2, respectively.

3.1. Polarimetric target decomposition

Polarimetric target decomposition is a frequently used technique to analyze the scattering characteristics of full polarimetric synthetic aperture radar (PolSAR) data (An and Lin, 2019; Wang et al., 2019). The polarimetric decomposition theory is mainly to take full advantage of the polarimetric information and better interpret radar data (Cloude and Pottier, 1996). The Yamaguchi decomposition method (Yamaguchi et al., 2005) is suitable for the complex geometric scattering structures such as snow due to its improvement in the nonreflection symmetric scattering case. Therefore, the GaoFen-3 and Radarsat-2 full-polarimetric data are processed by this method to obtain the surface (σ_Y^s), volume (σ_Y^v), double-bounce (σ_Y^{db}), and helix (σ_Y^h) scattering power. This process is done in the PIE-SAR software. The relationship between the total scattering power (σ^t) and the four components can be written as:

$$\sigma^t = \sigma_Y^s + \sigma_Y^v + \sigma_Y^{db} + \sigma_Y^h. \quad (2)$$

For wet snow, the double-bounce scattering and the helix scattering are small and hence can be neglected. The surface scattering, volume scattering, and local incidence angle maps (Fig. 4) with geographic coordinate information are obtained via the process of radiation calibration, multi-look, polarimetric speckle filtering, polarimetric decomposition, and geocoding. Due to the absorption of free liquid water in snowpack, the scattering value of snow-covered area is smaller and the color is darker than snow-free area on the map. Moreover, the surface scattering value is generally greater than the volume scattering value. More than 99.5% of the local incidence angle values in the two study areas are in the range of 5°–85°. The scattering value is inversely proportional to the local incidence angle value.

The polarimetric decomposition results obtained the proportions of the surface and volume scattering components under different states of snow (e.g. dry snow and wet snow), which provide the possibility to estimate the snow surface and volume wetness, and also provide the basis for effective snow wetness inversion under different snow conditions.

3.2. Extraction of backscattering coefficient

The extraction of radar backscattering coefficient mainly includes the process of radiation calibration, complex data conversion, multi-look, polarimetric speckle filtering, and geocoding. The HH polarization backscattering coefficient maps of GaoFen-3 and Radarsat-2 with geographic coordinate information are obtained by the above processing as shown in Fig. 5. These processes are also performed in the PIE-SAR software. Similarly, due to the influence of free liquid water in snowpack, the color of snow-covered area is darker than snow-free area on the backscattering coefficient map of HH polarization.

3.3. Simulation of snow surface scattering

According to the dominant scattering components in wet snow condition, the snowpack backscattering mainly contains two components:

$$\sigma_{pp}^t = \sigma_{pp}^s + \sigma_{pp}^v, \quad (3)$$

where pp represents the polarization.

Then the surface scattering can be expressed as:

$$\sigma^s = \sigma_{HH}^s + \sigma_{HV}^s + \sigma_{VH}^s + \sigma_{VV}^s. \quad (4)$$

According to the reciprocity relation, the amplitudes of cross-polarized scattering are identical in the backscattering direction, namely $\sigma_{HV}^s = \sigma_{VH}^s$ (Oh et al., 2002), then:

$$\sigma^s = \sigma_{HV}^s + 2\sigma_{HV}^s + \sigma_{VV}^s. \quad (5)$$

Because the radar parameters are determinate, the snow surface scattering can be expressed as:

$$\sigma^s = f(h, l, \theta, W_s), \quad (6)$$

where h, l, θ, and W_s represent the RMS height, correlation length, local incidence angle, and snow surface wetness, respectively.

Since the local incidence angle has been obtained during the polarimetric decomposition process, only the snow surface roughness and wetness are considered. According to the research by Zribi and Dechambre (2003), a smooth soil surface generally corresponds to a small value of h and a large value of l, and a ploughed soil often corresponds to a large h and a medium to large l. Moreover, taking two different values for h and l in the simulations can lead to the same backscattering value. Therefore, a combined roughness parameter, $Z_s = h^2/l$, was proposed. This turns two roughness parameters into one. In this work, we introduced the combined roughness parameter and thus the snow surface scattering can be expressed as:

$$\sigma^s = f(Z_s, W_s) \quad (7)$$

When we set a certain range of Z_s and W_s, the random rough surface scattering model can be used to simulate the surface scattering and

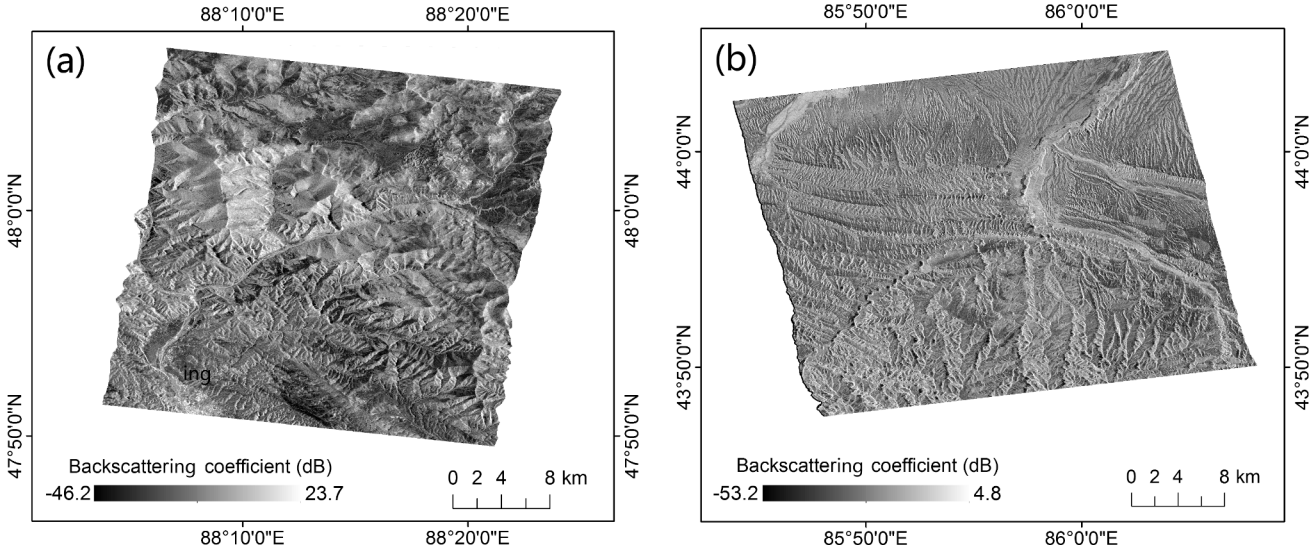

Fig. 5. Backscattering coefficient of HH polarization of GaoFen-3 (a) and Radarsat-2 (b) data.

establish the lookup table. The selection of the model and the parameters is also an important task, because the proper model and the parameters can not only improve the simulation accuracy but also improve the search efficiency.

The commonly used theory models for random rough surface scattering simulation include the physical optics model (POM), geometric optics model (GOM), small perturbation model (SPM), and integrated equation model (IEM) (Fung et al., 1992). Among them, the IEM can perform scattering simulation in a wide range of surface roughness, which can more truly represent the interaction process between the surface and the microwave. Chen et al. (2003) improved the IEM to make the simulation results more accurate. The improved model is called advanced IEM (AIEM). In addition, scholars have also established different empirical or semi-empirical models by using scatterometer measured datasets or theoretical model simulation datasets obtained under different ground condition, such as the Oh model (Oh et al., 1992), Dubois model (Dubois et al., 1995), and Shi model (Shi et al., 1997). In this study, the two study areas are located in the piedmont area, and the terrain of both areas is very undulating. Therefore, the AIEM with wider application range is selected to simulate σ^s_{HH} and σ^s_{VV}, and the Oh model is used to simulate σ^s_{HV} and σ^s_{VH}. σ^s can be obtained by adding σ^s_{HH}, σ^s_{VV}, σ^s_{HV}, and σ^s_{VH}. According to the previous studies (Shi, 2001; Shi and Dozier, 1995; Fassnacht et al., 2009), the terrain of the two study areas, and the range of local incidence angle, we set $\theta \in [5°, 85°]$, the step size is 1°, $Z_s \in (0, 0.2]$ cm, the step size is 0.002 cm, $W_s \in (0, 10]$ %, and the step size is 0.05%.

3.4. Simulation of snow volume scattering

Similar to Eq. (5), the volume scattering can be expressed as:

$$\sigma^v = \sigma^v_{HH} + 2\sigma^v_{HV} + \sigma^v_{VV}. \tag{8}$$

Separate σ^v_{HH} from the right side of Eq. (8), then:

$$\sigma^v = \sigma^v_{HH}\left(1 + \frac{\sigma^v_{VV}}{\sigma^v_{HH}} + \frac{2\sigma^v_{HV}}{\sigma^v_{HH}}\right) \tag{9}$$

Freeman and Durden's (1998) study shows that the cross-polarized component of volume scattering $\sigma^v_{HV} = \frac{1}{3}\sqrt{\sigma^v_{HH} \cdot \sigma^v_{VV}}$, then:

$$\sigma^v = \sigma^v_{HH}\left(1 + \frac{\sigma^v_{VV}}{\sigma^v_{HH}} + \frac{2}{3}\sqrt{\frac{\sigma^v_{VV}}{\sigma^v_{HH}}}\right) \tag{10}$$

Because snow is a kind of dense medium, the dense media radiative transfer theory developed by Tsang et al. (1985, 1992) can be used for simulating snow volume scattering. The first-order of snow volume scattering from an inhomogeneous dielectric half space medium is a function of the snow surface roughness, volume scattering albedo, local incidence angle, and permittivity:

$$\sigma^v_{pp} = \frac{3}{4}\omega T^2_{pp}\exp\left[-2h^2(k_1\cos\theta - k_2\cos\theta)^2\right], \tag{11}$$

$$T_{HH} = \frac{2\sqrt{\varepsilon - \sin^2\theta}}{\cos\theta + \sqrt{\varepsilon - \sin^2\theta}}, \tag{12}$$

$$T_{VV} = \frac{2\sqrt{\varepsilon - \sin^2\theta}}{\varepsilon\cos\theta + \sqrt{\varepsilon - \sin^2\theta}}, \tag{13}$$

where ω is the volume scattering albedo, which depends on snow particle size, density, wetness, size variation, and shape (Tsang et al., 1992). T_{pp} is either T_{HH} or T_{VV}, which is the Fresnel power transmission coefficients for vertical and horizontal polarization. The loss factor $\exp\left[-2h^2(k_1\cos\theta - k_2\cos\theta)^2\right]$ accounts for the snow surface roughness effect on the transmission. k_1 and k_2 are the real parts of the wave numbers in the layer and the incident medium, respectively (Ulaby, 1982; Fung, 1994). The local incidence angle θ should be converted into the local refractive angle using the Snell's law.

Assuming that the particles are spheres or randomly distributed, the volume scattering albedo is independent of the polarization. Therefore, different polarization ratio can eliminate the effect of the volume scattering albedo. Substitute Eq. (11) into Eq. (10):

$$\sigma^v = \sigma^v_{HH}\left(1 + \frac{T^2_{VV}}{T^2_{HH}} + \frac{2}{3}\sqrt{\frac{T^2_{VV}}{T^2_{HH}}}\right) \tag{14}$$

Then, substituting Eqs. (12) and (13) into Eq. (14) shows that the first-order volume scattering is only a function of dielectric constant, local incidence angle, and volume scattering of HH polarization. Since the local incidence angle has been obtained, the volume scattering function can be expressed as:

$$\sigma^v = f\left(\sigma^v_{HH}, \varepsilon\right), \tag{15}$$

where ε is the dielectric constant.

Hallikainen et al. (1986) established an empirical dielectric model by using the measured data. The model can describe the dielectric constant of snowpack when the frequency is 3–37 GHz, the wetness is 1–12%, and the density is 0.09–0.38 g/cm^3. The formula of real part is:

$$\varepsilon = A + \frac{B \cdot W^x}{1 + (f/f_0)^2}, \tag{16}$$

$$A = 1.0 + 1.83\rho + 0.02W^{1.015} + B_1, \tag{17}$$

$$B = 0.073A_1, \tag{18}$$

$$C = 0.073A_2, \tag{19}$$

$$x = 1.31, \tag{20}$$

where W, ρ, and f are the wetness, density, and frequency, respectively. f_0 is the relaxation frequency and$f_0 = 9.07$ GHz. When the frequency is 3–15 GHz, $A_1 = 1.0$, $A_2 = 0$, and $B_1 = 0$. When the frequency is 15–37 GHz, the expression of A_1, A_2, and B_1 are more complex. The specific expressions can be referred to the relevant literature (Hallikainen et al., 1986).

According to the measured average snow density, the snow density of the KRA and the MRA is set to 0.19 g/cm^3 and 0.32 g/cm^3, respectively. However, the density throughout the area is not uniform in fact. The effect of this difference on volume scattering simulation is discussed in detail in Section 5.1. When the density is determined, according to the Eqs. (16)–(20), the snow dielectric constant can be converted to wetness:

$$\sigma^v = f\left(\sigma^v_{HH}, W_v\right) \tag{21}$$

At this time, the volume scattering is only a function of σ^v_{HH} and W_v. Similar to the surface scattering simulation, when we set a certain range of σ^v_{HH} and W_v, the Eq. (21) can be used to simulate the volume scattering and establish the lookup table. Refer to the backscattering coefficient range of HH polarization in the snow-covered area, set $\sigma^v_{HH} \in (0, 0.02]$, and the step size is 2×10^{-5}. The range of local incidence angle and volume wetness is consistent with the surface scattering simulation.

4. Results

For the surface and volume scattering simulation, we analyzed the sensitivity of each parameter in the simulation process. Then based on the simulated results of surface and volume scattering, the surface wetness, volume wetness, and effective wetness were obtained in turn. Since the effective wetness is derived from the surface and volume wetness, it is necessary to analyze each component to ensure the accuracy of effective snow wetness.

4.1. Sensitivity of model parameters

We first analyzed the parameters Z_s and W_s in the surface scattering simulation. Under the premise of local incidence angle $\theta = 40°$, we set $W_s \in (0, 10]$ %, the step size is 0.4%, $Z_s \in (0, 0.2]$ cm, and the step size is 0.04 cm. The simulation result is shown in Fig. 6a. When Z_s is determined, the surface scattering increases with the increase of W_s, and the increasing rate decreases gradually. The difference between the maximum and minimum values is about 6 dB. When W_s is determined, as the increase of Z_s, the surface scattering also increases with the decrease of increasing rate. The difference between the maximum and minimum values is about 9 dB.

For the volume scattering simulation, we also set $\theta = 40°$, $W_s \in (0, 10]$ % with step size of 0.4%, and $\sigma^v_{HH} \in (0, 0.02]$ with step size of 0.004. σ^v_{HH} can be converted to a representation of dB. The simulation result is shown in Fig. 6b. When σ^v_{HH} is determined, as the increase of W_v, the volume scattering decreases steadily, and the difference between the maximum and minimum values is about 1 dB. When W_v is determined, the volume scattering increases with the increase of σ^v_{HH}, and the increasing rate also decreases gradually. The difference between the maximum and minimum values is about 7 dB.

4.2. Evaluation of snow surface wetness

The surface wetness was estimated using the surface scattering obtained by the polarimetric decomposition and the surface scattering lookup table established in Section 3.3, the results of surface wetness are shown in Fig. 7. Forest areas have been masked using the 30 m global land cover data (GlobalLand30) (Chen et al., 2015). The average surface wetness value of the KRA and the MRA is 5.80% and 4.79%, respectively. The surface wetness of the KRA is mainly concentrated at 4–10%, accounting for about 87% of the total area, of which 8–10% accounts for about 29%. This may be due to the thermal insulation of the thick snow layer in the KRA, which resulted in the high wetness of the bottom snow layer. This can refer to the analysis of field measurements in Section 4.4. At the same time, it is also an important reason that the average wetness in winter in the KRA is greater than that in spring in the MRA. From 0 to 10%, we set each range to 2%. The distribution of surface wetness in the MRA is relatively uniform in each range, and each range accounts for about 20% of the total area.

The absolute error between the simulated surface scattering and the surface scattering obtained by the polarimetric decomposition is calculated to evaluate the accuracy of the simulation. Since the scattering power values in the snow-covered area are almost in the range of 0.01–0.1, 0.001 is used as the standard of accuracy evaluation. The number of snow pixels in each range is counted. The statistical results are shown in Table 2. Among the 2,058,531 snow pixels in the KRA, there are 1,936,782 pixels with the absolute error of surface scattering power less than or equal to 0.001, accounting for 94.1% of the total snow pixels. Among the 2,045,551 snow pixels in the MRA, there are 1,973,543 pixels with the absolute error of surface scattering power less than or equal to 0.001, accounting for 96.5% of the total snow pixels. These results show that the absolute error of surface scattering power between the simulation and the polarimetric decomposition is mostly very small, which means that the surface wetness of the two study areas all have robust reliability.

4.3. Evaluation of snow volume wetness

Similar to the surface wetness inversion method, the volume scattering obtained by the polarimetric decomposition and the volume scattering lookup table established in Section 3.4 are used to estimate the volume wetness. The volume wetness results are shown in Fig. 8. The average volume wetness value of the KRA and the MRA is 5.15% and 4.39%, respectively. The volume wetness distribution in the KRA is relatively uniform, and the proportion of each wetness range is about 20%. In the MRA, the 0–2% volume wetness range accounts for about 30%, and the other wetness ranges each account for about 17%.

The absolute error of volume scattering power can also be obtained in the process of volume wetness estimation, that is, the absolute error between the simulated volume scattering and the volume scattering obtained by the polarimetric decomposition. Since the snow volume scattering power is mostly greater than 0.001, 0.0001 is used as the evaluation standard for the accuracy of the volume scattering simulation. The number of snow pixels in each range is counted. The statistical results are shown in Table 3. Among the 2,058,531 snow pixels in the KRA, there are 2,040,538 pixels with the absolute error of volume scattering power less than or equal to 0.0001, accounting for 99.1% of the total snow pixels. Among the 2,045,551 snow pixels in the MRA, there are 1,809,834 pixels with the absolute error of volume scattering power less than or equal to 0.0001, accounting for 88.5% of the total snow pixels. These results show that the absolute error of volume scattering power between the simulation and the polarimetric decomposition is mostly very small, which means that the volume wetness of the two study areas also have robust reliability.

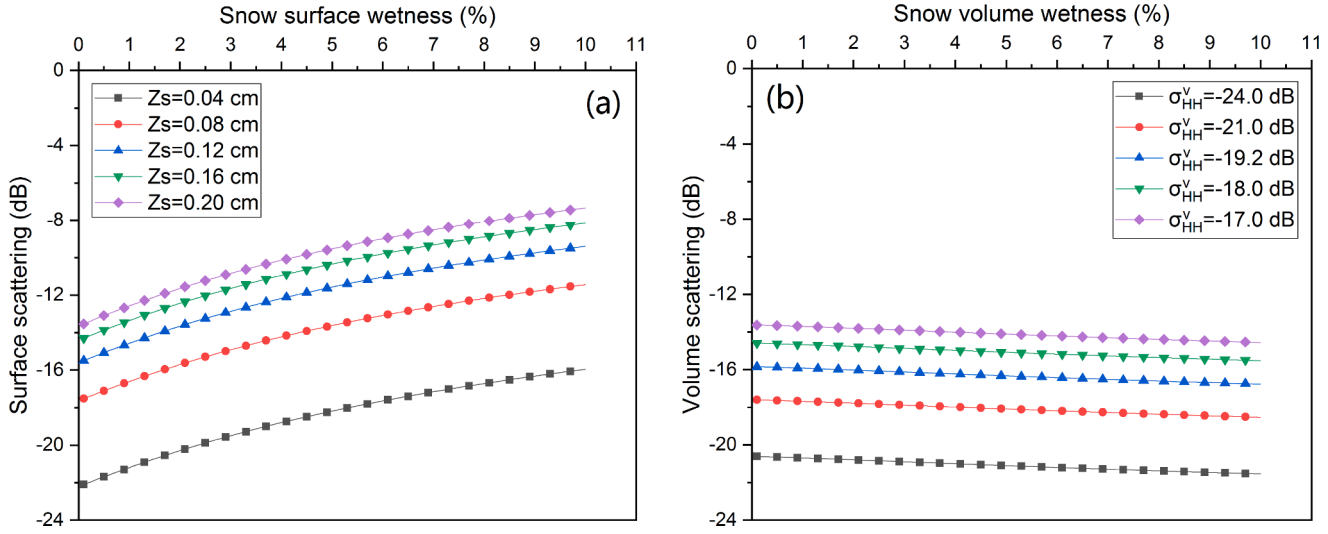

Fig. 6. Sensitivity of the model parameters. (a) shows the sensitivity of snow surface scattering to Z_s and W_s. (b) shows the sensitivity of snow volume scattering to σ^v_{HH} and W_v.

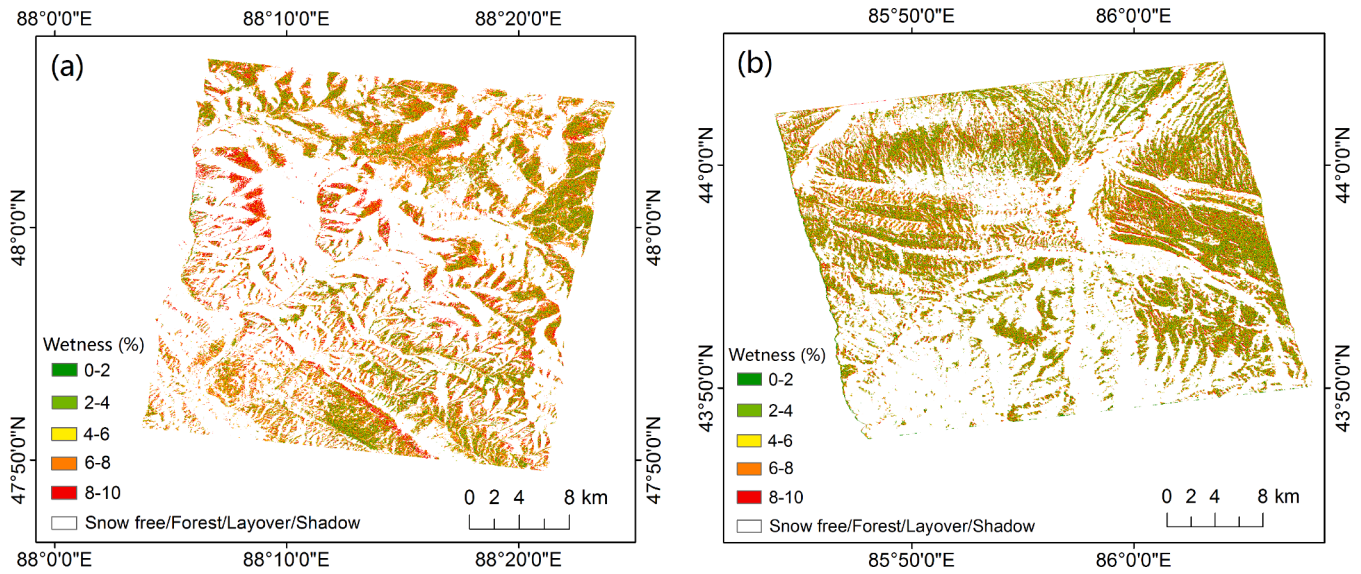

Fig. 7. Results of the snow surface wetness of the KRA (a) and the MRA (b).

Table 2
Absolute error distribution of the surface scattering power.

Data	Range	Pixel Number	Percentage (%)
GaoFen-3	$\lvert\sigma_Y^s - \sigma^s\rvert \le 0.001$	1,936,782	94.1
Radarsat-2	$\lvert\sigma_Y^s - \sigma^s\rvert \le 0.001$	1,973,543	96.5

4.4. Validation of effective snow wetness

The effective snow wetness obtained by weighted calculation is shown in Fig. 9. The average effective snow wetness value of the KRA and the MRA is 5.70% and 4.75%, respectively. The wetness range of 8–10 % account for about 22% in the KRA, and the higher surface wetness also leads to the higher effective snow wetness. In the MRA, about 78% of the wetness values are concentrated in the range of 2–8 %.

When verifying the inversion value with the measured data, it is necessary to consider comprehensively the wetness value and the penetration depth of C-band microwave. Therefore, we simulated the penetration depth of C-band under different snowpack density conditions (Fig. 10a) (Ulaby and Elachi, 1990). The effect of snow density on penetration depth is almost negligible, and the penetration depth depends mainly on the snow wetness. When the snow wetness is less than 1%, the C-band microwave can penetrate dozens of centimeters of snow. As the increase of snow wetness, the penetration depth decreases rapidly. When the snow wetness reaches 2%, the penetration depth is about 12 cm. When the snow wetness is in the range of 2–3%, C-band can only effectively obtain the snowpack information within 10 cm.

According to the field measurements, the snow depth of the KRA is larger, with a range of about 20–80 cm. The upper layer of snow is relatively dry, and the snow near the underlying surface is relatively

Table 3
Absolute error distribution of the volume scattering power.

Data	Range	Pixel Number	Percentage (%)
GaoFen-3	$\lvert\sigma_Y^v - \sigma^v\rvert \le 0.0001$	2,040,538	99.1
Radarsat-2	$\lvert\sigma_Y^v - \sigma^v\rvert \le 0.0001$	1,809,834	88.5

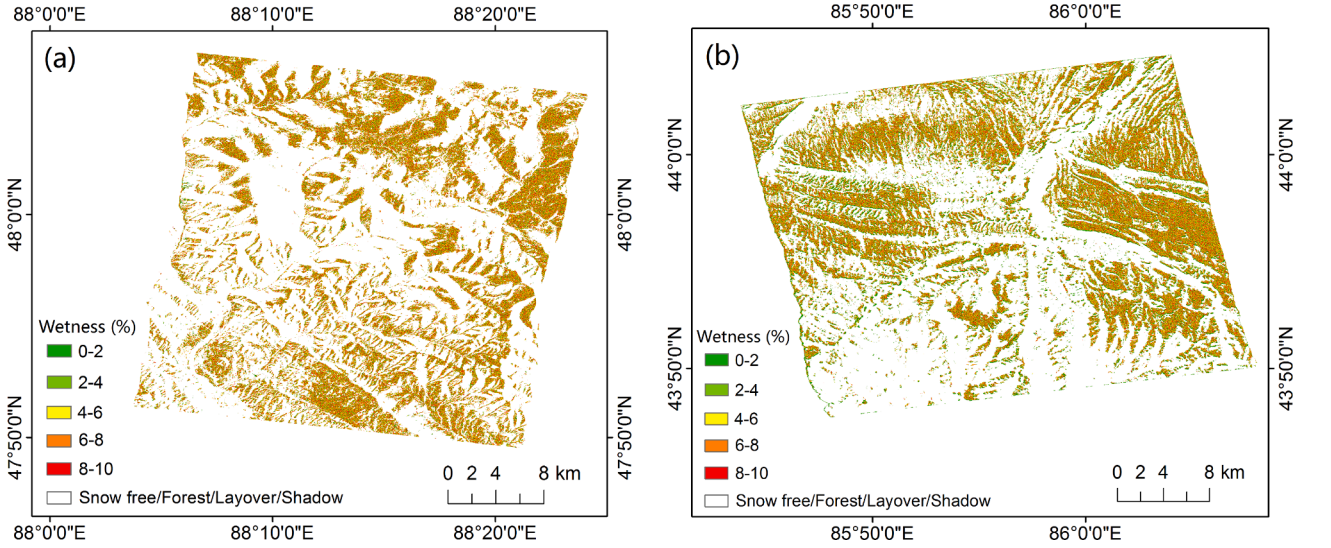

Fig. 8. Results of the snow volume wetness of the KRA (a) and the MRA (b).

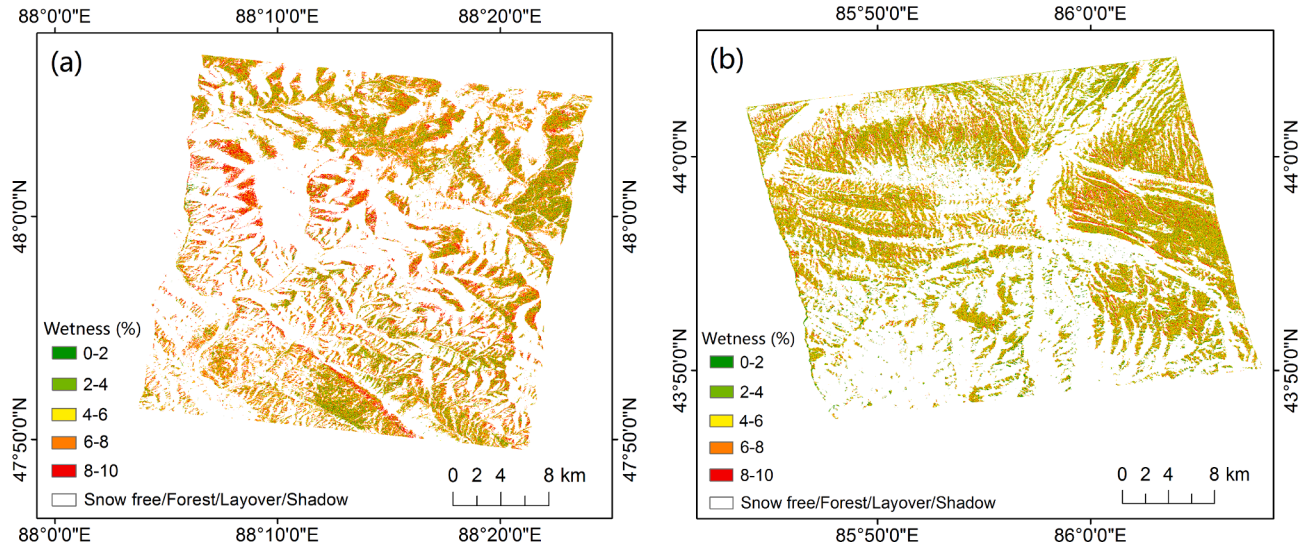

Fig. 9. Effective snow wetness of the KRA (a) and the MRA (b).

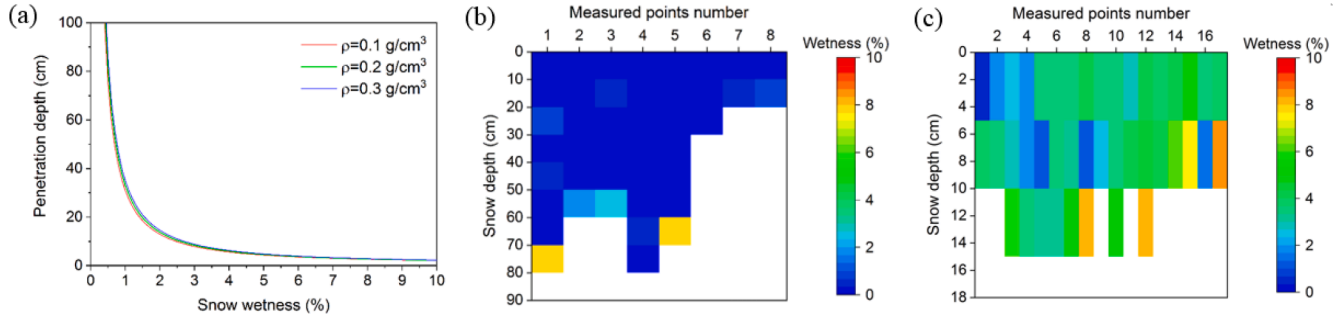

Fig. 10. Penetration depth of C-band microwave under different snow density and wetness (a), and snow depth and wetness of the field measurements in the KRA (b) and the MRA (c).

humid (Fig. 10b). The higher wetness value in each snow pit is used as the verification value. This is because the verification value should not only consider the wetness, but also consider the penetration depth of C-band microwave signal. At the same time, the snow above this layer is dry so as to ensure that the microwave reaches this layer under the premise of less influence by the upper snow layer. In the MRA, the snow depth is in the range of about 10–15 cm, and the wetness of the upper snow layer is relatively high (Fig. 10c). Therefore, the average snow wetness of around 10 cm in the upper layer is used as the validation value. The snow wetness of the KRA and the MRA estimated by the proposed method along with field measurements are plotted in Fig. 11.

The correlation coefficient (R) between the proposed method results and the field measurements in the KRA is 0.72, and the mean absolute error (MAE) and the root mean square error (RMSE) are 3.35% and

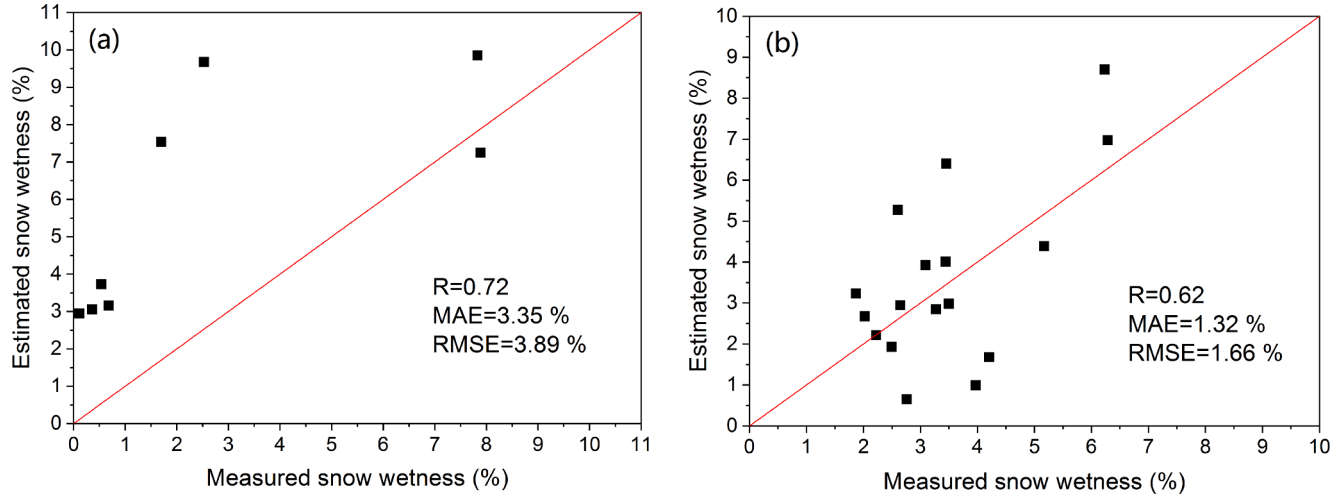

Fig. 11. Validation of the GaoFen-3 (a) and Radarsat-2 (b) estimated snow wetness along with field measurements of KRA and MRA, respectively.

3.89%, respectively. The proposed method results have been overestimated to some extent, especially when the snow wetness is low. The main reasons are as follows: (1) when the snow wetness is low, the microwave penetration depth is large, and it can even reach the underlying surface. The backscattering of dry snow is similar to that of bare ground. With the increase of snow wetness, the SAR backscattering will decrease rapidly due to the absorption of microwave by water (Baghdadi et al., 1997; Mätzler, 1987). Therefore, due to the influence of underlying surface, the measured points with low wetness will cause the increase of backscattering, which will lead to the large estimation value of snow wetness; and (2) when verifying the estimated value with the field measurements, considering that the upper layer of snow wetness is low, and the microwave can penetrate, while the snow near the underlying surface is relatively humid and the microwave is difficult to penetrate, the snow wetness of this layer is hence used as the validation value. However, when the depth of the snow is large, the snow on the upper layer will inevitably have a certain influence on the backscattering. At this time, if only the snow wetness of the underlying snow layer is used as the validation value, the true wetness of the whole snow layer is underestimated, which results in the large estimated value of the proposed method.

The correlation coefficient between the proposed method results and the field measurements in the MRA is 0.62, and the MAE and the RMSE are 1.32% and 1.66%, respectively. Because of the higher wetness of the upper snowpack in this area, the estimated value will not be affected by the underlying surface and the upper snowpack. Compared with the field measurements, the estimated values do not appear larger.

4.5. Comparison with the Shi-Dozier model

Using R, MAE, and RMSE as three evaluation indicators, the proposed method was compared with the Shi-Dozier model (Shi and Dozier, 1995) (Table 4). Shi-Dozier model is the development of Shi 93 model (Shi et al., 1993). It considers the influence of snow surface roughness. The backscattering of wet snow proposed by this model mainly comes from the surface scattering at the air-snow interface and the volume scattering of the snow layer, which can be regarded as the theoretical basis for snow wetness inversion. Therefore, the classic Shi-Dozier model is selected for comparison with the proposed model.

It can be seen from Table 4 that the inversion results based on the proposed model achieve higher accuracy than those of the Shi-Dozier model for the GaoFen-3 and Radarsat-2 data. This can be attributed to the fact that the proposed model takes into account both the ground conditions of the study area and the role of cross-polarization terms in snow wetness inversion. In addition, the possible reason for the negative correlation between the GaoFen-3 estimated results and the field measurements is that the Shi-Dozier model is more suitable for areas with high snow wetness.

5. Discussion

In the previous section, we analyzed the reliability of the snow surface, volume wetness, and effective snow wetness estimated results, which shows that the proposed method has strong applicability in different areas and periods. However, the estimation of the wetness is also subjected to various sources of uncertainty following from the assumptions made for developing the method. Therefore, these uncertainty sources are discussed below.

Table 4
Comparison of the proposed method with the Shi-Dozier model.

	Data	R	MAE (%)	RMSE (%)
Proposed method	GaoFen-3	0.72	3.35	3.89
	Radarsat-2	0.62	1.32	1.66
Shi-Dozier model	GaoFen-3	−0.32	3.58	4.36
	Radarsat-2	0.37	5.33	5.97

5.1. Uncertainty of the snow density

In the process of volume scattering simulation, we assumed that the value of snow density parameter is fixed. However, the snow density is not uniform throughout the areas, which results in the uncertainty of the volume scattering (Shi and Dozier, 2000). Fig. 12 shows the effect of snow density on the volume scattering and the snow density of the field measurements in two study areas. With the increase of density, the volume scattering decreases. The reduced volume scattering is about 1 dB when the density reaches 0.6 g/cm^3. According to the field measurements in the KRA, the minimum and maximum density values are 0.098 and 0.3 g/cm^3, respectively. The simulated volume scattering with minimum and maximum density differs by 0.32 dB. In the MRA, the measured minimum and maximum densities are 0.14 and 0.571 g/cm^3, respectively. The corresponding volume scattering differs by 0.56 dB.

However, because the density distribution of the entire area cannot be obtained, we are unable to obtain the volume scattering error distribution. Moreover, it is necessary to calculate the absolute error of volume scattering between the simulation and the polarimetric decomposition to obtain the volume wetness. The volume and surface wetness are multiplied by their respective weights and then adding them together to obtain the effective snow wetness. Therefore, the deviation caused by density to effective snow wetness is even more uncertain.

5.2. Uncertainty of the ground condition

Although both study areas have achieved reliable estimates, there are still some differences between them. For example, the correlation between the estimated results and the field measurements in the KRA is better, but the MAE and RMSE are larger than the MRA. Fig. 13 shows the typical ground conditions of the two study areas. The snow depth in the KRA is greater than the MRA, and even some areas around the measured points are covered with no snow in the MRA. Moreover, the terrain in the KRA is relatively flat, and the MRA is rugged. Thus, the mixed pixels and the complex terrain caused a decrease in the correlation between the estimated results and the field measurements in the MRA.

On the other hand, because the snow wetness in the KRA is relatively small, the underlying surface has a greater impact on backscattering. As a result, the MAE and RMSE in this area are higher than the MRA. At this time, the influence of the underlying surface on the wetness estimation is also difficult to evaluate. In addition, when the underlying surface type is relatively dense vegetation, the influence of the branches on the radar signal cannot be ignored. Therefore, the uncertainty of the wetness caused by the underlying surface requires further study.

6. Conclusion

In this study, we proposed a new method to estimate snow wetness from full-polarimetric SAR data. This method fully considered the snow surface roughness and local incidence angle on complex mountain terrain and the polarimetric information of the SAR data. In addition, we chose the GaoFen-3 data obtained on January 17, 2018 in the Kelan River Basin and the Radarsat-2 data obtained on March 19, 2014 in the Manasi River Basin to estimate the snow wetness. There were differences in the acquisition date, location, snow conditions, satellite orbits, and sensors between the two types of SAR data. These differences could be used as the evaluation standard for the applicability of the proposed method on various conditions. By performing the proposed method, the estimated results were verified by using near-synchronous ground observation data. It was found that the deviations between the estimated results of the two types of data and the measured values were small, which proved the reliability of the proposed method. However, the uncertainty of snow wetness estimated results caused by the snow

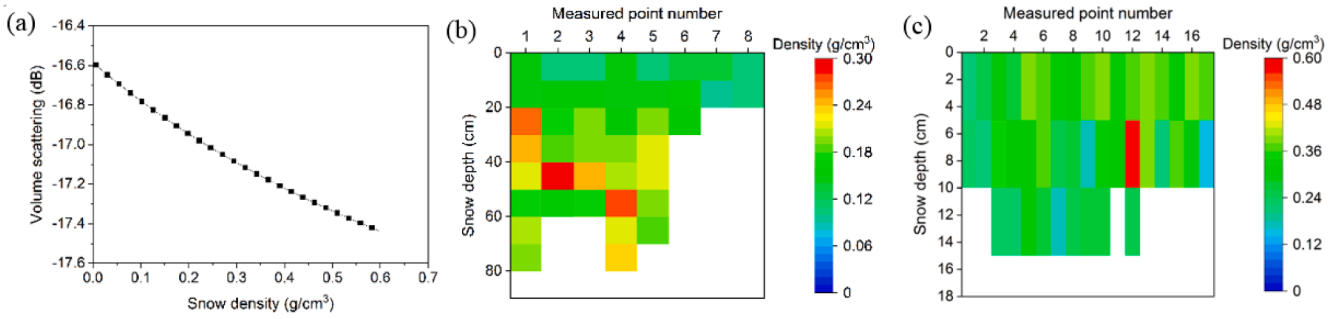

Fig. 12. Volume scattering as a function of snow density (a), and the snow density of the field measurements in the KRA (b) and the MRA (c).

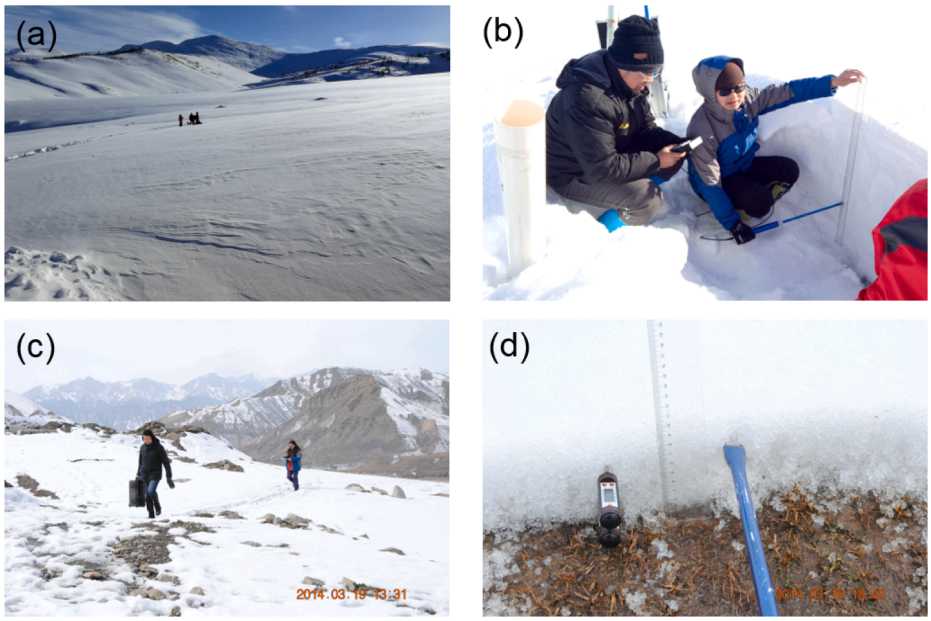

Fig. 13. Ground conditions of the KRA (a and b) and the MRA (c and d).

density and ground conditions is still unsolved. Due to this, the proposed method will be further improved.

Declaration of Competing Interest

The authors declare that they have no known competing financial interests or personal relationships that could have appeared to influence the work reported in this paper.

Acknowledgements

This work was supported by the National Natural Science Foundation of China under Grant No. 41671344, the Science & Technology Basic Resources Investigation Program of China under Grant No. 2017FY100502, and the Postgraduate Research & Practice Innovation Program of Jiangsu Province under Grant No. KYCX20_0030. The authors thank the China Centre for Resources Satellite Data and Application for the kindly providing the GaoFen-3 data. They thank the Piesat Information Technology Co., Ltd. for providing the PIE-SAR software authorization code. They also thank the field observers who obtained the valuable near-synchronous field measurements from the two study areas.

References

An, W., Lin, M., 2019. A reflection symmetry approximation of multilook polarimetric SAR data and its application to Freeman-Durden decomposition. IEEE Trans. Geosci. Remote Sens. 57, 3649–3660.

Baghdadi, N., Gauthier, Y., Bernier, M., 1997. Capability of multitemporal ERS-1 SAR data for wet-snow mapping. Remote Sens. Environ. 60, 174–186.

Bhattacharya, A., Surendar, M., De, S., Venkataraman, G., Singh, G., 2014. Snow wetness estimation from dual polarimetric coherent TerraSAR-X data, in: 2014 IEEE Geoscience and Remote Sensing Symposium (IGARSS), Quebec City, pp. 2766–2769.

Chen, J., Chen, J., Liao, A., Cao, X., Chen, L., Chen, X., He, C., Han, G., Peng, S., Lu, M., Zhang, W., Tong, X., Mills, J., 2015. Global land cover mapping at 30m resolution: A POK-based operational approach. ISPRS J. Photogramm. Remote Sens. 103, 7–27.

Chen, K.S., Wu, T.D., Tsang, L., Li, Q., Shi, J., Fung, A.K., 2003. Emission of rough surfaces calculated by the integral equation method with comparison to three-dimensional moment method simulations. IEEE Trans. Geosci. Remote Sens. 41, 90–101.

Cloude, S.R., Pottier, E., 1996. A review of target decomposition theorems in radar polarimetry. IEEE Trans. Geosci. Remote Sens. 34, 498–518.

Cui, Y., Xiong, C., Shi, J., 2017. Estimation of snow wetness by a dual-frequency radar, in: 2017 IEEE International Geoscience and Remote Sensing Symposium (IGARSS), Fort Worth, pp. 1363–1365.

Dubois, P.C., Van Zyl, J., Engman, T., 1995. Measuring soil moisture with imaging radars. IEEE Trans. Geosci. Remote Sens. 33, 915–926.

Fassnacht, S.R., Stednick, J.D., Deems, J.S., Corrao, M.V., 2009. Metrics for assessing snow surface roughness from digital imagery. Water Resour. Res. 45, W00D31.

Freeman, A., Durden, S.L., 1998. A three-component scattering model for polarimetric SAR data. IEEE Trans. Geosci. Remote Sens. 36, 963–973.

Fung, A.K., Li, Z., Chen, K.S., 1992. Backscattering from a randomly rough dielectric surface. IEEE Trans. Geosci. Remote Sens. 30, 356–369.

Fung, A.K., 1994. Microwave scattering and emission models and their applications. Artech House, Boston, MA, USA.

Hallikainen, M., Ulaby, F., Abdelrazik, M., 1986. Dielectric properties of snow in the 3 to 37 GHz range. IEEE Trans. Antennas Propag. 34, 1329–1340.

Mätzler, C., 1987. Applications of the interaction of microwaves with the natural snow cover. Remote Sens. Rev. 2, 259–387.
Oh, Y., Sarabandi, K., Ulaby, F.T., 1992. An empirical model and an inversion technique for radar scattering from bare soil surfaces. IEEE Trans. Geosci. Remote Sens. 30, 370–381.
Oh, Y., Sarabandi, K., Ulaby, F.T., 2002. Semi-empirical model of the ensemble-averaged differential Mueller matrix for microwave backscattering from bare soil surfaces. IEEE Trans. Geosci. Remote Sens. 40, 1348–1355.
Rondeau-Genesse, G., Trudel, M., Leconte, R., 2016. Monitoring snow wetness in an Alpine Basin using combined C-band SAR and MODIS data. Remote Sens. Environ. 183, 304–317.
Shi, J., Dozier, J., Rott, H., 1993. Deriving snow liquid water content using C-band polarimetric SAR. In: in: 1993 IEEE International Geoscience and Remote Sensing Symposium (IGARSS), pp. 1038–1041.
Shi, J., Dozier, J., 1995. Inferring snow wetness using C-band data from SIR-C's polarimetric synthetic aperture radar. IEEE Trans. Geosci. Remote Sens. 33, 905–914.
Shi, J., Wang, J., Hsu, A.Y., O'Neill, P.E., Engman, E.T., 1997. Estimation of bare surface soil moisture and surface roughness parameter using L-band SAR image data. IEEE Trans. Geosci. Remote Sens. 35, 1254–1266.
Shi, J., Dozier, J., 2000. Estimation of snow water equivalence using SIR-C/X-SAR. I. Inferring snow density and subsurface properties. IEEE Trans. Geosci. Remote Sens. 38, 2465–2474.
Shi, J., 2001. A numerical simulation of estimating snow wetness with ASAR. In: in: 2001 IEEE International Geoscience and Remote Sensing Symposium (IGARSS), pp. 922–924.
Singh, G., Kumar, V., Mohite, K., Venkatraman, G., Rao, Y.S., Snehmani, 2006. Snow wetness estimation in Himalayan snow covered regions using ENVISAT-ASAR data, in: 2006 International Society for Optics and Photonics (SPIE), Goa, pp. 641008.
Singh, G., Venkataraman, G., 2007. Snow wetness mapping using advanced synthetic aperture radar data. J. Appl. Remote Sens. 1, 013521.
Singh, G., Venkataraman, G., 2010a. Snow wetness retrieval inversion modeling for C-band and X-band multi-polarization SAR data. In: in: 2010 IEEE International Geoscience and Remote Sensing Symposium (IGARSS), pp. 4664–4667.
Singh, G., Venkataraman, G., 2010b. Snow permittivity retrieval inversion algorithm for estimating snow wetness. Geocarto Int. 25, 187–212.
Surendar, M., Singh, G., Bhattacharya, A., Venkataraman, G., Bharathi, P.A., 2013. Snow wetness estimation based on Pol-SAR decomposition technique. In: in: 2013 IEEE International Geoscience and Remote Sensing Symposium (IGARSS), pp. 3199–3202.
Surendar, M., Bhattacharya, A., Singh, G., Yamaguchi, Y., Venkataraman, G., 2015. Development of a snow wetness inversion algorithm using polarimetric scattering power decomposition model. Int. J. Appl. Earth Obs. Geoinformation 42, 65–75.
Tsang, L., Kong, J.A., Shin, R.T., 1985. Theory of microwave remote sensing. John Wiley and Sons, New York.
Tsang, L., Ding, K.H., Wen, B., 1992. Dense media radiative transfer theory for dense discrete random media with particles of multiple sizes and permittivities. Prog. Electromagn. Res. 6, 181–225.
Ulaby, F.T., 1982. Microwave remote sensing: Active and passive, Volume 2. Artech House, Boston, MA, USA.
Ulaby, F.T., Elachi, C., 1990. Radar polarimetry for geoscience applications. Artech House, Boston, MA, USA.
Wang, H., Magagi, R., Goïta, K., Trudel, M., McNairn, H., Powers, J., 2019. Crop phenology retrieval via polarimetric SAR decomposition and random forest algorithm. Remote Sens. Environ. 231, 111234.
Xiao, P., Feng, X., Xie, S., Du, J., 2015. Research progress of high-resolution remote sensing of snow in Manasi River Basin in Tianshan Mountains. Xinjiang Province. J. Nanjing Univ. (Natural Sci.) 51, 909–920.
Yamaguchi, Y., Moriyama, T., Ishido, M., Yamada, H., 2005. Four-component scattering model for polarimetric SAR image decomposition. IEEE Trans. Geosci. Remote Sens. 43, 1699–1706.
Yu, Q., Shi, J., Shao, Y., Liu, W., 2004. Modeling of snow wetness inversion using multi-polarization SAR at C-Band, in. In: 2004 IEEE International Geoscience and Remote Sensing Symposium (IGARSS), pp. 3696–3699.
Zhuo, Y., Xiao, P., Feng, X., Zhang, X., Yang, Y., Ye, L., Li, C., Hu, R., Bian, G., 2017. Spatial distribution and features of the snow cover during accumulation period in the middle reaches of the Kelan River, Altay region. Xinjiang. J. Glaciol Geocryol. 39, 979–988.
Zribi, M., Dechambre, M., 2003. A new empirical model to retrieve soil moisture and roughness from C-band radar data. Remote Sens. Environ. 84, 42–52.